ACS APPLIED NANO MATERIALS

Article

Inkjet-Printed Carbon Nanotube Electrodes Modified with Dimercaptosuccinic Acid-Capped Fe3O4 Nanoparticles on Reduced Graphene Oxide Nanosheets for Single-Drop Determination of Trifluoperazine

Milos Ognjanovic, Dalibor M. Stankovi#, Milica Jovic, Milena Krsti#, Andreas Lesch, Hubert H. Girault, and Bratislav V. Antic

ACS Appl. Nano Mater., **Just Accepted Manuscript** • DOI: 10.1021/acsanm.0c00661 • Publication Date (Web): 22 Apr 2020

Inkjet-Printed Carbon Nanotube Electrodes Modified with Dimercaptosuccinic Acid-Capped Fe_3O_4 Nanoparticles on Reduced Graphene Oxide Nanosheets for Single-Drop Determination of Trifluoperazine

Miloš Ognjanović [†,*], Dalibor M. Stanković[†], Milica Jović[‡], Milena P. Krstić[§], Andreas Lesch[ǂ], Hubert H. Girault[‡] and Bratislav Antić[†]

[†]The "Vinča" Institute of Nuclear Sciences, University of Belgrade, POB 522, 11001 Belgrade, Serbia

[‡]Laboratory of Physical and Analytical Electrochemistry (LEPA), EPFL Valais Wallis, Rue de l'Industrie 17, CH-1951 Sion, Switzerland

[§]Faculty of Veterinary Medicine, University of Belgrade, Belgrade, Serbia

[ǂ]Department of Industrial Chemistry "Toso Montanari", University of Bologna, Viale del Risorgimento 4, 40136 Bologna, Italy

***Keywords**: disposable sensor; magnetite; graphene nanocomposite; square wave voltammetry; CNT electrodes*

Abstract

Here we report the design of a disposable single-drop voltammetric sensor for the quantitative determination of antipsychotic drug trifluoperazine (TFP). The sensor was build using inkjet-printed carbon nanotube (CNT) electrodes which were modified with dimercaptosuccinic acid (DMSA) coated magnetite nanoparticles uniformly dispersed over reduced graphene oxide nanosheets (DMSA/Fe_3O_4/RGO). The used modifying materials were characterized by electron microscopies (TEM and FE-SEM), X-ray powder diffraction, zeta potential measurements, DLS and electrochemical methods (CV and EIS). Developed sensor, best operated at pH 7 in Britton-Robinson buffer solution (BRBS), shown linear electrocatalytic activity in the concentration range from 1 to 50 μM TFP, with a low detection limit of 0.54 μM and excellent selectivity, repeatability and reproducibility with RSD of 2.4%. A voltammetric approach using the square wave voltammetry (SWV) was used as a sensitive technique under optimized conditions for the analytical determination of sub-micromolar amounts of TFP. Bare CNT, RGO- and DMSA/Fe_3O_4-modified CNT resulted in a less electrocatalytic activity then DMSA/Fe_3O_4/RGO/CNT electrode. The development of this kind of TFP sensor based on nanoparticles decorated graphene nanosheets can offer a tool for point-of-care applications of the sensor in biomedicine.

Introduction

Trifluoperazine (10-[3-(4-methyl-1-piperazinyl)propyl]-2-(trifluoromethyl)-10*H*-phenothiazine) is a dopamine antagonist with antipsychotic and antiemetic activities mainly used for schizophrenia treatment [1]. TFP is one of the most potent antipsychotic phenothiazine-type drugs that express its antipsychotic effect by blocking central dopamine receptors and prevent effects such as delusions and hallucinations caused by an excess of dopamine. This agent also functions as a calmodulin inhibitor, thereby leading to the elevation of cytosolic calcium. Trifluoperazine was also reported to be superior as a placebo for the treatment of generalized anxiety disorder [2] and as an inhibitor of cancer stem cell growth [3]. As TFP is highly metabolized by the liver and eliminated with urine there has been a need for a new method for the detection of this drug in biological fluids and pharmaceuticals. Considering the structure of the trifluoperazine (**Scheme 1**) its electrochemical nature should be distinctively determined by phenothiazine core and the appointed piperazine ligand [4].

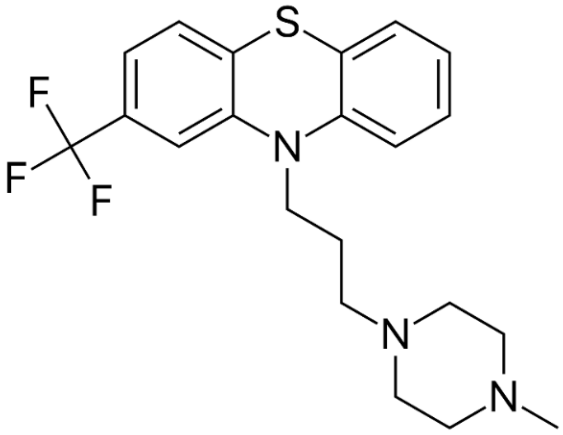

Scheme 1. 10-[3-(4-methyl-1-piperazinyl)propyl]-2-(trifluoromethyl)-10*H*-phenothiazine, (TFP).

The clinical method for TFP determination by the United States Pharmacopeia is volumetric nonaqueous titration with perchloric acid, which requires a large number of drug samples and organic solvents [5]. Considering the electrochemical methods, which can significantly make impact on this area, only few have been reported so far, based on boron-doped diamond electrode [6], poly-aminobenzene sulphonic acid/single-walled carbon nanotubes composite-modified glassy carbon electrode [7], multi-walled carbon nanotube-modified glassy carbon [8], and aminobenzene sulphonic acid/single-wall carbon nanotubes/glassy carbon electrode [9]. The main aim of this work was designing a new droplet-based electrochemical sensor based on graphene nanocomposite with improved performances toward TFP determination. Nanoparticles decorated graphene were frequently used for surface modification of the working electrode in building new sensors [10].

Functionalized graphene materials have attracted much attention in electrochemical sensors due to the exciting properties, such as high surface area and electron transport under ambient conditions which makes them promising candidates for the implementation in portable sensors [11,12]. Graphene (GR), a flat monolayer of sp^2-bonded carbon atoms tightly packed into a two-dimensional honeycomb lattice, is considered as one of the thinnest materials on Earth [13,14]. Graphene oxide (GO) is one of the most important derivatives of graphene and possesses enormous surface area, reasonable conductivity depending on the degree of oxidation and great mechanical properties. It is used in various fields such as energy materials, biosensing, catalysis and biomedicine [15]. Furthermore, it is difficult to disperse GR in polar solvents due to its hydrophobicity. On the other side, GO contains hydrophilic groups, such as -OH, -COOH, -O–C=O, and =C=O, and can, therefore, be homogeneously dispersed together with active materials, like commonly used metal oxides, in a polar matrix for its deposition onto the electrode surfaces. In GO, the π-network and thus the electronic conductivity is lower compared to GR. Therefore, GO cannot directly be used as a conductive electrode material so that it needs to be reduced to reduced graphene oxide (RGO) under regeneration of the π-network [16].

On the other side, magnetic nanomaterials and especially iron oxide nanoparticles (IONPs) are one of the most dynamic and fast-growing areas of research in the field of nanotechnology [17–19]. The properties of IONPs differ significantly from the iron oxide bulk counterpart and depend on several factors, such as composition, surface area, shape, size, surface morphology and anisotropy. Among possible materials for surface modifications of IONPs, dimercaptosuccinic acid (DMSA), a small organic molecule, has been widely used to form aqueous suspensions and provide better dispersity of nanoparticles and consequently higher surface area [20]. Furthermore, the decoration of graphene-based materials by bare or surface-modified IONPs has become a hot topic due to their enhanced functionalities [21,22]. At that way fabricated graphene-based nanocomposites holds a great promise for designing an electrochemical sensor that has a wide variety of applications such as biomedical fields, catalysis, removal of contaminants from wastewater, biosensors, etc. [23–25]. Achieved functionalities are due to combined or the synergistic effect of enhancing electron transfer rates and active surface conductivity by increasing the specific surface area and promoting transition.

Disposable inkjet-printed carbon nanotube electrodes are a recently developed type of electrodes with many desirable properties, like high conductivity, droplet detection, small active area and good mechanical strength of the employed CNTs [26–28], which makes them attractive for flexible nanoelectronics devices [29]. After modification of CNT with carbon-based nanocomposites, their performance could be further enchanted so these electrodes have the potential to be a great starting point for the production of small flexible sensors for point-of-care (POC) electronic devices [30,31].

Herein we report the fabrication and application of a sensitive and highly selective disposable droplet-based electrochemical sensor for the detection of TFP in biological fluids. Uniform iron oxide magnetic nanoparticles with a controlled core diameter of 13 nm have been synthesized by thermal decomposition of an iron oleate complex in 1-octadecene. The synthesized nanoparticles were coated with DMSA for better dispersibility in polar solvents and spread over the sheets of reduced graphene oxide (DMSA/Fe_3O_4/RGO). The proposed nanocomposite was further used for the modification of inkjet-printed CNT electrodes and applied for the detection of TFP.

Experimental section

Reagents

All reagents were used as obtained and without any further treatment. For the synthesis of nanocomposite DMSA/Fe_3O_4/RGO commercial products, iron(III) chloride hexahydrate (98%, Sigma-Aldrich), sodium oleate (82%, Riedel-de Haen), oleic acid (90%, Aldrich), 1-octadecene (90%, Sigma-Aldrich), n-hexane (99%, Scharlau), toluene (99.8%, Sigma-Aldrich), meso-2,3-dimercaptosuccinic acid (DMSA, ~98%, Sigma Aldrich), dimethyl sulfoxide (DMSO, ≥99%, Sigma Aldrich), graphene oxide sheets (Sigma-Aldrich), ethylene glycol (≥99.5%, Fluka Analytical) and ammonium hydroxide solution (28% NH_3 in H_2O, ≥99.99%, Sigma-Aldrich) were used. The following materials were used for the fabrication of the inkjet-printed carbon nanotube electrodes: disposable ink of nano-silver: Silverjet DGP-40LT-15C (w/w 30-35%, Sigma Aldrich), CNT dispersion (Brewer Science), jettable insulator EMD6201 (Sun Chemical) and hypochlorite solution (ACROS Organics, available chlorine 5%).

Synthesis of DMSA/Fe_3O_4/RGO nanocomposite

Uniform iron oxide magnetic nanoparticles were synthesized by thermal decomposition of an iron oleate complex in 1-octadecene by controlling nucleation and growth processes using slightly modified procedure described in ref. [32]. Briefly, the iron oleate complex was synthesized by measuring 45 g of sodium oleate and 10.8 g of $FeCl_3.6H_2O$ and mixing them with distilled water (60 mL), absolute ethanol (80 mL) and n-hexane (140 mL) inside a 1-neck round-bottomed flask. The suspension was heated for 4 hours at 70 °C under magnetic stirring and after cooling to room temperature (RT) the solution was poured into a separation funnel and the phases were separated by washing with a mixture of ethanol and water. Once the washing procedure has been completed and the last aqueous layer was removed, the top layer containing the iron oleate complex was transferred to the single neck round-bottomed flask. All the solvents were removed with the help of a rotary evaporator. The amount of 4.5 g of iron oleate complex prepared in the previous section was transferred to a 3-neck round bottom flask, mixed with 50 mL of 1-octadecene and placed on an electro mantle under mechanical stirring with a blanket of nitrogen. The temperature program was set to reach 315 °C (± 5 °C), maintained for 1 hour and allowed to cool down to RT. Then, nanoparticles were precipitated with absolute ethanol, centrifuged and finally dispersed in 25 mL of toluene.

To get a better dispersion of the nanoparticles, the procedure of their surface modification was conducted according to the one described in ref. [33]. The nanoparticles were coated with DMSA by mixing 5 mL of toluene nanoparticle stock with 90 mg of meso-2,3-dimercaptosuccinic acid and 5 mL of dimethyl sulfoxide followed by 10 min processing in an ultrasonic bath. The system was placed on the rotator and the solution was mixed at 10-20 rpm for 48 hours. The supernatant was decanted and the precipitate was centrifuged and washed three times with ethanol and allowed to dry for 24 hours in the air.

In the last step of nanocomposite synthesis, the DMSA coated iron oxide nanoparticles were used for decorating graphene oxide (GO) sheets. For this, 5 mg of the synthesized iron oxide nanoparticles were mixed with 1.5 mL of GO suspension (5 mg·mL^{-1}) in 25 mL of ultra-pure MiliQ water under 4 h of magnetic stirring while a uniform suspension was achieved. The pH value of the suspension was adjusted to about 10 by the addition of NH_4OH. After that, the mixture was sonicated for 1 h at RT. Then, the suspension was heated at 160 °C for 10 min using a microwave synthesis reactor (Anton Paar, Monowave 300, Austria) followed by cooling inside of the reactor to RT. The black precipitate was centrifuged and washed with deionized water several times and finally re-dispersed in 5 mL of dimethylformamide (DMF). For the sake of comparison, RGO was also obtained by reduction from GO by direct microwave-assisted irradiation. It has been shown that GO can be reduced to RGO with the help of microwave irradiation [34]. The process of nanocomposite synthesis is shown graphically on the **Scheme 2A**.

Characterization techniques

The crystal structure properties were analyzed by the use of X-ray powder-diffraction (XRPD) data. The measurements were performed on a high-resolution Smart Lab® X-ray diffractometer (Rigaku, Japan) equipped with Cu Kα radiation source (λ = 0.1542 nm). The collected data were in 10° to 75° 2θ range with the conditions as follows: a step of 0.05°, exposition of 2 s per step, the divergent slit of 0.5 mm, operating at 40 kV and 30 mA.

Microstructure and morphology of synthesized samples were investigated using a transmission electron microscope JEOL-JEM 1010 (JEOL, Japan) operating at 100 kV, and field emission-scanning electron microscope FE-SEM MIRA3 (Tescan, Czech Republic) operating at 30 kV. The sample was prepared by placing a drop of particles suspended in water onto a carbon-coated copper grid and allowing them to dry at RT for FE-SEM and TEM observations. The TEM images were analyzed manually by ImageJ software [35]. The mean particle size and distribution were evaluated by measuring the largest internal dimension of 300 nanoparticles. Afterwards, the data were fitted to a log-normal function ($y = y_0 + \frac{A}{\sqrt{2\pi}\omega x} e^{\frac{-\left[\ln\frac{x}{xc}\right]^2}{2\omega^2}}$) to obtain the mean size and standard deviation (σ) and index of polydispersity (PdI), which is considered to be representative of the absolute error of the measurement.

The zeta potentials of a 0.1 mg/mL suspension of naked and DMSA coated samples dispersed in deionized water were measured at 25±0.1°C in disposable zeta cells (DTS 1070) of a NanoZS90 (Malvern, UK) device. Samples were performed after 30 min of equilibrium at a constant ionic strength of 0.01 M set by NaCl. The hydrodynamic particle size by dynamic light scattering (DLS) was determined on a NanoZS90 apparatus (Malvern, UK) with a 4 mW He-Ne laser source (λ=633 nm). The stock sols of two samples were diluted to a concentration of 0.1 mg mL^{-1}. The pH was varied between 2 and 12 by addition of HNO_3 and KOH. All measurements were performed at a given kinetic state followed by a minute of relaxation. The average values of the hydrodynamic diameter were calculated as the number weighted size from fits of the correlation functions. The pH measurements were performed using Lab pH meter InoLab® (WTW, Germany) with a combined glass electrode (SenTix® 41).

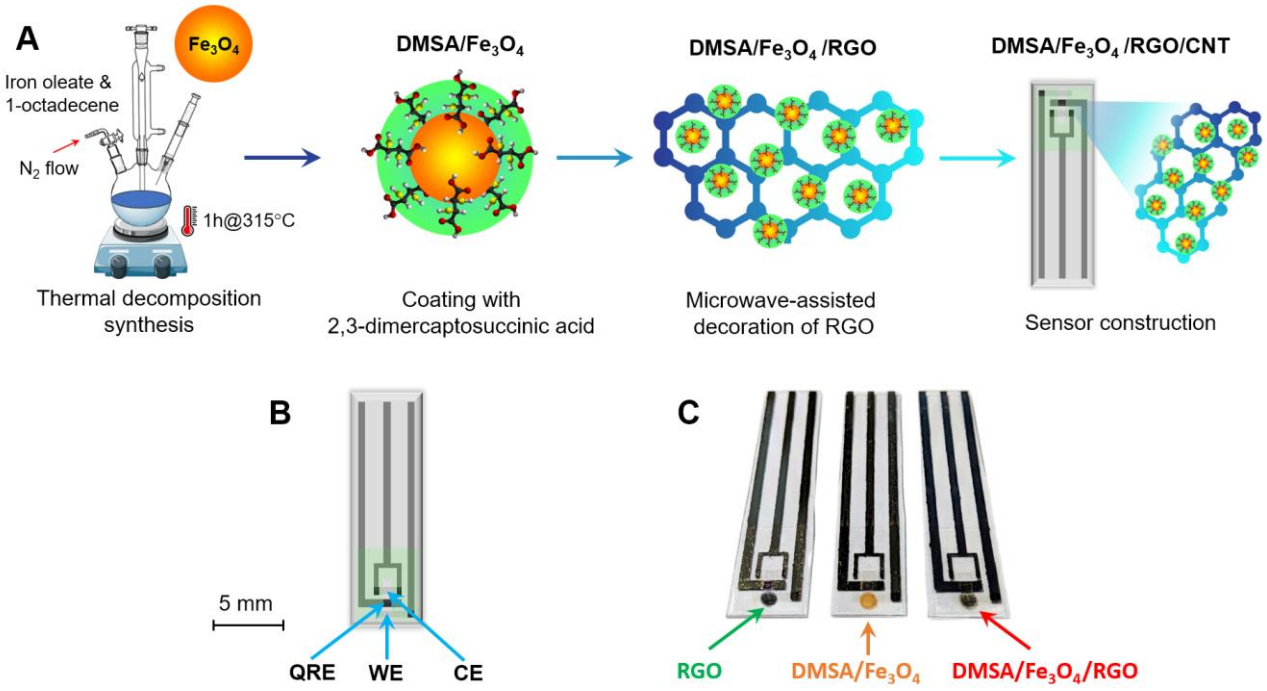

Scheme 2. (A) The synthesis of DMSA/Fe_3O_4/RGO nanocomposite and modification of CNT electrode (B) Schematic illustration of CNT electrode (QRE, WE and CE denote quasi-reference electrode, a working electrode and counter electrode, respectively); (C) Photographs of three modified electrodes by drop-casting 2 µL of materials on working electrode.

Electrochemical experiments were executed with help of Autolab potentiostat model 302 N (Autolab PGSTAT302N, Metrohm, Netherlands) in a three-electrode arrangement system with a working electrode (WE), a counter electrode (CE) and a reference electrode (RE). The experiments were performed in 0.1 M Britton-Robinson buffer solution at pH 7. Electrochemical impedance spectroscopy (EIS) measurements were performed in the presence of a stationary 5 mM $K_3[Fe(CN)]_6/K_4[Fe(CN)]_6$ (1:1) mixture as a redox probe in 0.1 M KCl solution with the frequency changed from 100 Hz to 100 kHz with a signal amplitude of 5 mV at a potential of 0.05 V. The scan rate in cyclic voltammetry was 50 $mV \cdot s^{-1}$.

Fabrication of the inkjet-printed carbon nanotube (CNT) electrodes and modified CNT electrodes

Inkjet-printed carbon nanotube electrodes were produced on PET substrates (thickness 180 µm) with protocol precisely defined elsewhere [36–38]. Briefly, the electrodes were printed using an X-Serie Cera inject-printer (CeraDrop, France) armed with piezoelectric Dimatix Q-class Sapphire QS-256–80pL print-heads and disposable DMC-11610 cartridges. As a first layer, jettable nanosilver ink was imprinted and cured as an electrical connection layer and quasi-reference electrode material. The second printed material was a CNT dispersion used for the fabrication of CNT patterns to form standalone working and counter electrodes. The third layer was insulator that was printed and at the same time UV-photopolymerized, making an insulation layer on top of the silver-lines and specifically designating all operating electrode surfaces (WE-CNT, QRE-Ag, CE-CNT), of about 1 mm^2 each. Finally, the silver electrode was converted into an Ag/AgCl quasi-reference electrode chemically by exposing the silver electrode surface to hypochlorite solution, and at the end washing with water [38,39].

The graphical illustration of the CNT electrode, as well as photographs of already prepared sensors, are given in **Scheme 2**. The more in-depth schematic construction of CNT electrodes layer by layer could be found in detail in our previous works [31,36]. Briefly, it is presented at **Scheme 2B**.

To prepare DMSA/Fe_3O_4/RGO/CNT electrodes, the synthesized DMSA/Fe_3O_4/RGO powder was dried, dissolved in DMF (5 $mg \cdot mL^{-1}$) and sonicated for 3 h. After this period, 2 µL of the composite solution was deposited on the carbon nanotube working electrode (WE-CNT) and allowed to dry at RT. DMSA/Fe_3O_4/RGO/CNT electrodes were further dried overnight at +4 °C. As working electrodes, bare CNT, DMSA/Fe_3O_4-, RGO- and DMSA/Fe_3O_4/RGO-modified CNT electrodes were used and compared.

Samples for testing modified CNT – detection of TFP

Human urine samples were obtained from four healthy and young people (female and male). The urine samples were prepared according to our previous work [40]. Before use, samples were stored in a refrigerator at + 4 °C and the samples were spiked with a standard solution of TFP on the day of the measurements. Additionally, the blood serum samples of two healthy volunteers were acquired from the local hospital. After the centrifugation, 1 mL of supernatant was added to 0.8 mL acetonitrile and stirred for 45 s. The obtained mixture was centrifuged at 15,000 rpm for 10 min. After the centrifugation, different volumes of obtained supernatant were directly analyzed. The samples were spiked with a standard solution of the TFP. The recovery studies for both, urine and blood serum, were carried out. Results are calculated from the calibration curve and summarized as a mean value of three independent measurements.

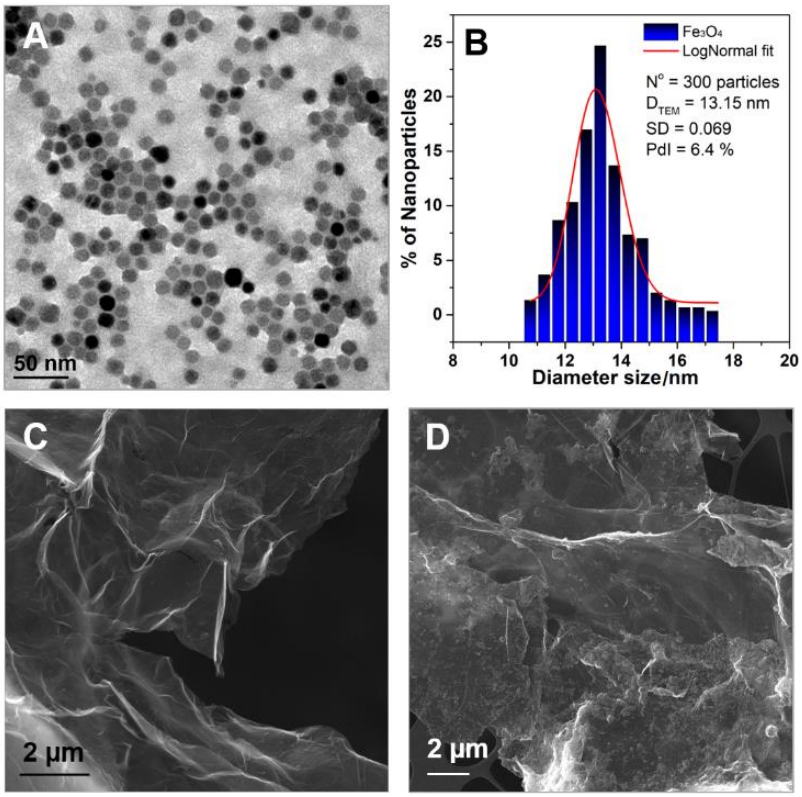

Figure 1. (A) TEM micrograph of DMSA coated Fe_3O_4 nanoparticles. Scale bar is 50 nm; (B) Log-normal size distribution of iron oxide nanoparticles; FE-SEM micrographs of (C) GO and (D) DMSA/Fe_3O_4/RGO nanocomposite.

Results and discussion

Structural characterization of nanoparticles and nanocomposite

Crystal structure and microstructure of magnetite nanoparticles and nanocomposite were examined by X-ray diffraction technique and electron microscopies (TEM and FE – SEM). Thanks to the thin DMSA surface layer surrounding the nanoparticles, they were less agglomerated and thus well dispersed. The TEM micrographs of synthesized nanoparticles are shown in **Figure 1A**. As illustrated, these nanoparticles were mainly spherical, well dispersed and uniform in size, d_{TEM} = 13.1 ± 0.8 nm. The nanoparticles undergo log-normal size distribution with a PdI index of 6.4% (**Figure 1B**). The surface morphology of GO and DMSA/Fe_3O_4/RGO was observed using FE-SEM. **Figure 1C** reveals an almost transparent single layer of GO which possesses a large surface area. There are many wrinkles and creases on the folded surface of GO to reduce surface energy making it more stable. The small magnetite nanoparticles are scattered over the surface of RGO sheets further enhancing the surface area, as displayed in **Figure 1D**. These results indicate that the nanoparticles are firmly and homogeneously dispersed to the RGO nanosheets with a vital influence on the surface of the nanocomposite that was beneficial for the electrochemical processes (see below)[41,42]. The crystal structure of DMSA/Fe_3O_4, GO, RGO and DMSA/Fe_3O_4/RGO was checked by X-ray powder diffraction technique (**Figure 2A**). The reflections of synthesized DMSA/Fe_3O_4 *(orange line)* can be ascribed to spinel structure type, space group Fd-3m (No. 227), matching the most intensive diffraction peaks with simulated diffraction data (JCPDS Card #19-629). The crystallite size estimated by the Debye-Scherrer equation of the most intensive reflection (311) gave the result of d_{XRPD} = 9.49 nm and agreed well with d_{TEM} suggesting high crystallinity of the nanoparticles. The sharp diffraction peak at 10.25° matched well with the (002) reflection of GO *(blue line)*. This peak turned into a broad peak at 22.5° of 2θ after the microwave synthesis *(green line)*. This is a confirmation of the successful reduction of GO to RGO [43]. Accordingly, the XRPD pattern of the DMSA/Fe_3O_4/RGO *(red line)* suggests that in the course of the microwave-assisted hydrothermal synthesis highly dispersed nanocrystals of Fe_3O_4 become anchored to the RGO sheets generated from the GO reduction during synthesis. RGO sheets generated from the GO reduction during the synthesis.

Well-established method for the surface modification of nanoparticles is important to see if the coating procedure is performed successfully. The constructed zeta potential *vs* pH curves for uncoated and DMSA coated Fe_3O_4 NPs are shown in **Figure 2B**. The successful coating process can be confirmed by the reduction of the isoelectric point (the zero of particle's charge) from pH 7.6 to pH 3.6, and by slight reduction of the surface charge. The addition of the carboxylic group-rich dimercaptosuccinic acid to the suspension of Fe_3O_4 that is rich with positive ions of $Fe^{2+/3+}$ on the surface NPs had an apparent effect on the zeta potential of the nanoparticles, making the dispersion more stable at

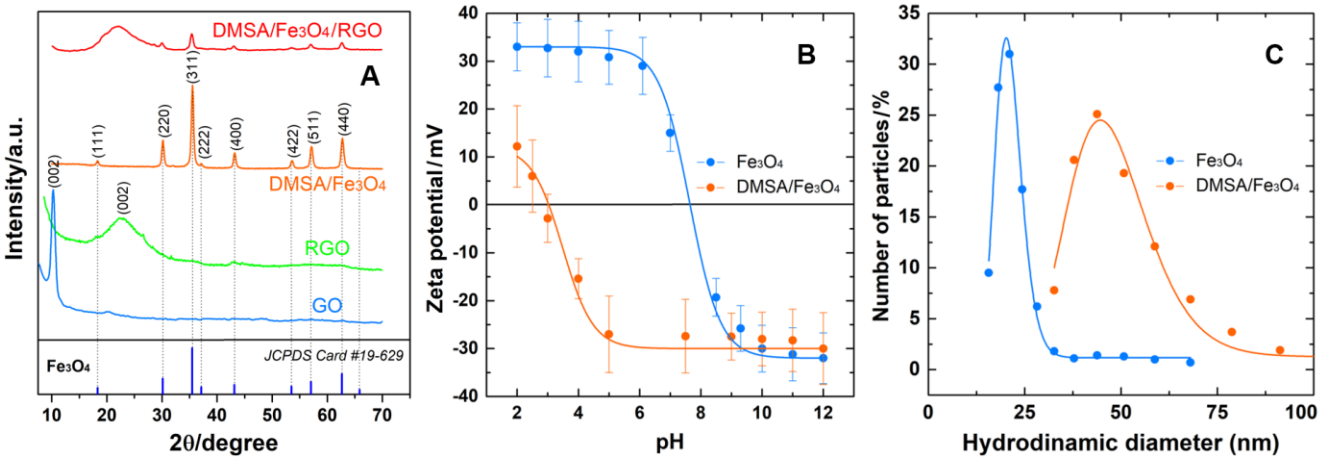

Figure 2. (A) XRPD patterns of the synthesized samples: GO (blue line), RGO (green line), DMSA/Fe_3O_4 nanoparticles (orange line) and DMSA/Fe_3O_4/RGO composite (red line). For comparison, a typical Fe_3O_4 pattern (JCPDS card #19-629) was displayed in the figure; B) The effect of pH on zeta potential of naked and DMSA coated Fe_3O_4 nanoparticles; (C) Hydrodynamic diameter of uncoated and coated nanoparticles.

physiological pH. The Coulomb electrostatic repulsion forces are the key to the assembly process and DMSA/Fe_3O_4 coating. The effect of coating procedure on the hydrodynamic size (D_H) of particles, measured by DLS, is given in **Figure 2C**. The D_H values increased from 20.8 nm for naked Fe_3O_4 to 46.9 nm for DMSA-coated Fe_3O_4 nanoparticles showed that the outer shell of dimercaptosuccinic acid is stacked over magnetite nanoparticles. It must be noted that D_H represents the diameter of particles in their hydrated state in water dispersion and, therefore, the values are higher than D_{TEM}, given the different nature of the particle's sizes.

Electrochemical performance of the proposed sensor

The electrocatalytic activity of unmodified and modified CNT electrodes toward electrochemical detection of 75 μM of TFP was examined using cyclic voltammetry at pH 7 of Britton-Robinson buffer (BRBS) with a scan rate of 50 mV·s^{-1}. **Figure 3A** shows changes in oxidation currents that display electrocatalytic behavior of bare and differently modified CNT electrodes. As it can be seen, TFP shows an oxidation peak with $E_{1/2}$ potential of around 0.63 V. The RGO-modified CNT electrode *(green line)* increased the oxidation peak of CNT electrode *(blue line)* from 0.75 μA to 0.8 μA, while the DMSA/Fe_3O_4-modified CNT electrode *(orange line)* increased the current to 1 μA. The experimental result shows that when DMSA/Fe_3O_4/RGO were deposited over the CNT electrode *(red line)* the current increased more than 4 times, which could be due to a faster electron transfer rate. This can be credited to the increasing capability of diffusion and active surface area of the electrode. The use of the inkjet-printed CNT electrode was beneficial due to the miniaturized sensor dimensions compared to standard screen-printed electrodes (SPCE), which resulted in 25 times lower amounts of analyte per analysis (as low as 2-5 μL^{-1})[31].

To investigate the electron transfer capabilities of different electrodes, AC impedance experiments were carried out.

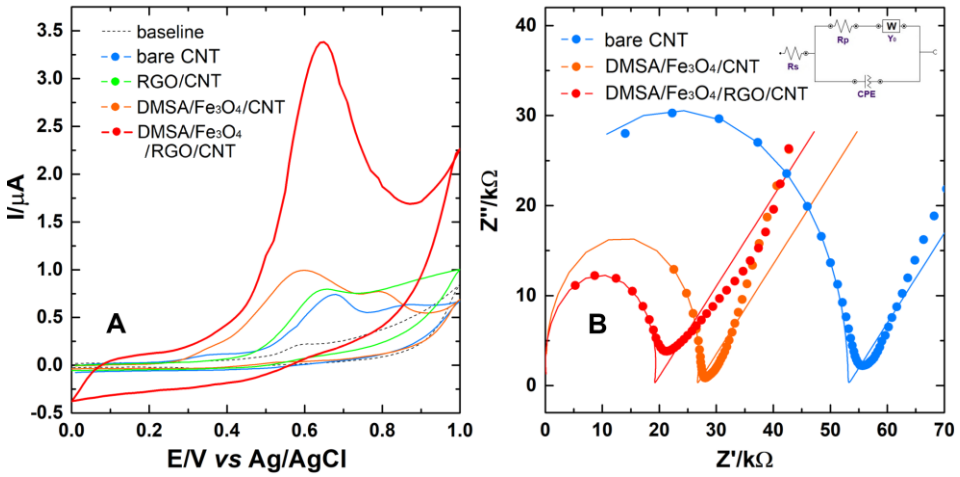

Figure 3. (A) Electrochemical response of TFP (75 μM) at bare CNT, DMSA/Fe_3O_4-, RGO- and DMSA/Fe_3O_4/RGO-modified CNT electrodes. Supporting electrolyte BRBS at pH 7, scan rate 50 mV·s^{-1}; (B) Nyquist plots for various electrodes, bare CNT, RGO-DMSA/Fe_3O_4- and DMSA/Fe_3O_4/RGO-modified CNT. Inset: Equivalent circuit for the electrochemical impedance spectroscopy data. The frequency range was from 100 Hz to 100 kHz.

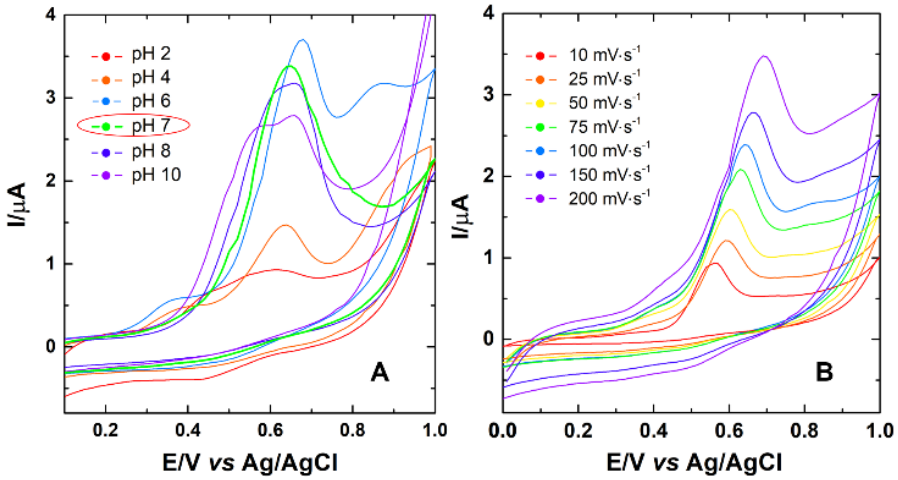

Figure 4. (A) Cyclic voltammograms of TFP (75 μM) at DMSA/Fe_3O_4/RGO-modified CNT electrode at various pH of BRBS. Scan rate 50 mV·s^{-1}; (B) Cyclic voltammograms of TFP (75 μM) at DMSA/Fe_3O_4/RGO-modified CNT electrode at various scan rates. Supporting electrolyte BRBS pH 7.

EIS measurements were performed since EIS is an effective and sensitive tool for the characterization of the interface properties of an electrode surface during each modification step. The obtained Nyquist diagrams at the different electrodes are shown in **Figure 3B**. In the Nyquist plot, the electron transfer resistance (R_{ct}) on the sensor surface is related to the diameter of the semicircle. According to the results, the bare CNT electrode showed the highest semicircle diameter. More than 55 kΩ indicates a slow electron transfer process for 5 mM $Fe(CN)_6^{3-/4-}$ as a redox probe. The smallest semicircle diameter at ~20 kΩ of the DMSA/Fe_3O_4/RGO/CNT indicated that the modification of the CNT layer with DMSA/Fe_3O_4/RGO decreased the electron transfer resistance of the interface. On the other hand, a larger R_{ct} value of DMSA/Fe_3O_4/CNT of about 28 kΩ, and 50 kΩ and for RGO/CNT indicated that the combination of RGO and Fe_3O_4 on the sensing surface was essential for good sensor performance. The experimental impedance data were further fitted using an equivalent electrical circuit fit tool in the NOVA 2 software package (Metrohm Autolab). Several models of circuits to fit our experimental data were attempted. The best results (best agreement between experiment and fitting for all three electrodes) were obtained with the equivalent circuit presented as an inset of **Figure 3B**.

The dynamic surface area of bare and modified electrodes was calculated using the Randles-Sevcik equation. The CV technique was used to measure 1.0 mM $K_3[Fe(CN)_6]$ as a test analyte and 0.1 M KCl was used as supporting electrolyte at different scan rates at 25 °C (**Figure S1**). The equation (1) was used to calculate the surface area of the electrode:

$$I_p = (2.69 \cdot 10^5)\, n^{3/2} A D_0^{1/2} v^{1/2} c_0^* \qquad (1)$$

where n is the number of electrons involved in the reaction i.e., equal to 1, A is effective area of electrode, D_0 is diffusion coefficient (for $K_3[Fe(CN)_6]$ is 7.6×10^{-6} cm^2 s^{-1}), v is scan rate and c_0^* is concentration of $K_3[Fe(CN)_6]$ (1.0 mM). From the slope of the plot, $I_p = f\left(v^{\frac{1}{2}}\right)$ the effective surface area of the bare electrode was found to be 0.041 cm^2 for pure five

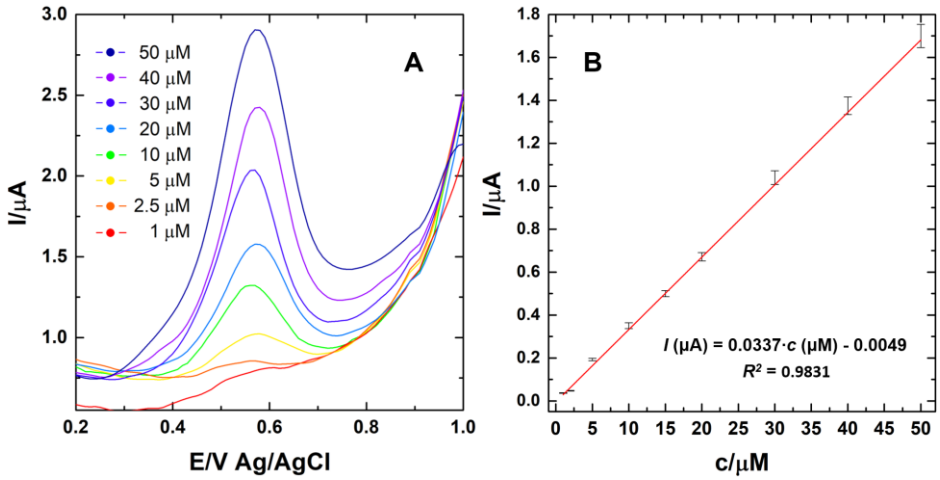

Figure 5. (A) SWV voltammograms obtained with DMSA/Fe_3O_4/RGO/CNT electrode for the concentration range of TFP from 1 to 50 μM, pH = 7; (B) Corresponding calibration plot evaluated from the measurements. All experiments were conducted under previously optimized experimental conditions.

times higher (0.285 cm^2). s for TFP, it can lose two electrons in the oxidation process. If two electrons were lost together in two steps, there were two anodic peaks, like in the case of bare CNT electrode. But under the condition with DMSA/Fe_3O_4/RGO nanocomposite, apparently, two electrons were lost in one step, thus only one peak appeared [7].

Selection of supporting electrolyte pH and the effect of the scan rate

For the study pH values effect of the supporting electrolyte (**Figure 4A**) cyclic voltammetry was used. A constant increase in the peak currents with pH was noticed in Britton-Robinson buffer solution, reaching the maximum at pH 7. After pH 7 the currents were slightly decreasing, but the spreading of the peaks was also observed. This may be due to favorable oxidation of resembling molecules in acid environments, by the reaction: R-OH + $2H^+$ + $2e^-$ → R-OH· and generation of polymer compounds, typical for polyphenols [44]. Consequently, BRBS at pH 7 was chosen as a basic electrolyte for further experiments. Additionally, cyclic voltammograms of the same concentration of TPF at pH 7 were recorded at various scan rates to examine the nature of the process that is taking place at the surface of the modified electrodes (**Figure 4B**). The increase of the scan rate was followed by an increase in the oxidative peaks currents. The peak currents were linearly increasing with the scan rate square root as seen in **Figure S2A** indicating that the process is diffusion controlled. The corresponding linear equation for oxidation process was I (μA) = $0.091 \cdot v^{1/2}$ $(mV/s)^{1/2}$ + 0.343 with a regression coefficient of 0.9981. Similarly, the dependency of log I *vs.* log v was linearly described by the equation log I = 0.344·log v - 0.588 and a regression coefficient of 0.9987 (**Figure S2B)**. Given the above results, it was clear that the processes dominant at the working electrode surface are diffusion controlled. A small movement of the peak potentials could be credited to the minor contribution of processes that are controlled by adsorption.

Based on Laviron's theory, a number of electrons involved in the electrochemical oxidation can be calculated using the equation (2):

$$I_p = n^2F^2vA\Gamma_0^*/4RT = nFQv/4RT. \quad (2)$$

From this equation, electron number (n) can be calculated as long as the peak current (I_p), and peak area (Q) are obtained under a certain scan rate (v). According to the equation (2), n was calculated to be 1.4, meaning two electrons were involved in electrochemical oxidation, which is in accordance with other reported values [7].

Square wave voltammetry detection of TFP

For the quantification of TFP, square wave voltammetry (SWV) was chosen. To boost sensitivity and selectivity of the suggested method, different conditions were varied, such as amplitude (tested range 10-100 mV), frequency (5-50 Hz) and potential step (2-15 mV). While one parameter was varied the others were kept constant. The obtained optimum values were: amplitude 60 mV, frequency 5 Hz and 10 mV as a step of potential. The calibration plot was composed with the consecutive addition of a TFP standard solution. The SWV response of DMSA/Fe_3O_4/RGO/CNT electrode toward different standard solutions of TFP and the corresponding calibration graph was plotted in **Figure 5A** and **5B**. Given the graph linear range of 1-50 μM was obtained under optimal conditions. The linear equation of this dependence is I (μA) = 0.0337·c (μM) - 0.0049 with a correlation coefficient of 0.9831. The detection limit (LOD, 3 $sd_{intercept}$/slope) of TFP using the DMSA/Fe_3O_4/RGO/CNT sensor was 0.54 μM, while the quantification limit (LOQ, 10 $sd_{intercept}$/slope) was 1.79 μM. The obtained linear range (0.4-20.4 mg/L) is well beyond the C_{max} value of TFP (15-20 mg/day) which falls into the upper end of our detection limit. The obtained results are comparable with few alternative sensors found in the literature [6,7,9]. As it can be seen in **Table 1**, in comparison with already reported TFP sensors in biological samples, the electroanalytical data of here constructed sensor were comparable, especially in the part of the linear range. Other than that, using this construction of the working electrode only one drop (2-5 μL) of sample solution was needed for analysis, which is very attractive for point-of-care applications.

For the determination of the reproducibility of the designed sensor, 10 μM TFP was analyzed with six identically modified electrodes under the same SWV conditions. All of the sensors were stored in the refrigerator at + 4 °C for a few days before use. The relative standard deviation for the detected peak currents obtained from the measurements was calculated to be 2.4% (n = 6) as an indicator of the sensor's precision (**Figure S3** and **Table S1**). Given these results, the sensor fabrication process is highly reproducible and sensors are successfully used for TFP concentration determination.

Table 1. Comparison of the TFP sensors reported in the literature

Electrode	Detection method	Linear range (μM)	Detection limit (μM)	Reference
BDD[a]	DPV	1-37	0.6	6
ABSA/SWNT/GCE[b]	DPV	0.1-10	0.001	7
MWCNT/GCE[c]	Ad-SDPV	0.02-1.67	0.0007	8
MCP-MWCNT/CPE[d]	SWV	0.5-1340	0.110	9
DMSA/Fe_3O_4/RGO/CNT	SWV	1-50	0.54	*This work*

[a]BDD – boron-doped diamond electrode; [b]ABSA/SWNT/GCE – aminobenzene sulphonic acid/single-wall carbon nanotubes/glassy carbon electrode; [c]MWCN T/GCE – multiwalled carbon nanotubes/glassy carbon electrode; [d]MCP-MWCNT/CPE – m-cresol purple-MWCNT-carboxylated multiwalled carbon nanotubes/carbon paste electrode.

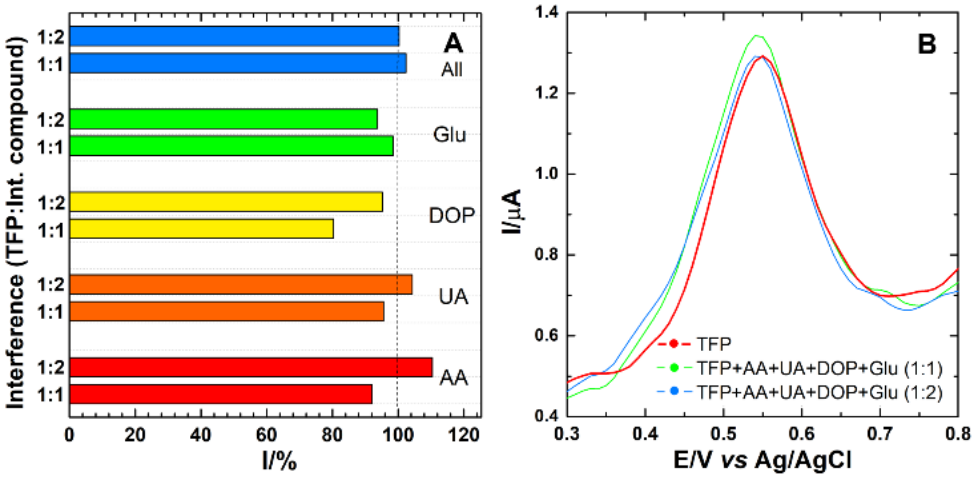

Figure 6. (A) Electrochemical response of TFP (10 μM) at DMSA/Fe_3O_4/RGO/CNT electrode in the presence of interfering compounds: ascorbic acid (AA), uric acid (UA), dopamine (DOP) and glucose (Glu) in concentration ration 1:1 and 1:2 v/v under optimized experimental conditions; (B) SWVs of the interference of all compounds combined.

Interferences analysis and real sample analysis

Before testing the practical applicability of the proposed method in real samples, the interfering effect of some ordinary compounds, which could be found in biological fluids, was examined. The sensor's selectivity was validated in the presence of ascorbic acid (AA), uric acid (UA), dopamine (DOP) and glucose (Glu) and all four combined (AA+UA+DOP+Glu), resembling possible interfering molecules (**Figure 6**). The measured concentration ratio between TFP (10 μM) and the molecules analyzed for interference in all examined conditions were 1:1 and 1:2. It was found that only DOP reduced the oxidation current for TFP slightly to 80% under the selected electrochemical window. The difference between interfered peaks was about 135 mV. In all other situations, the changes in current were significantly less than 10%. The electrochemical response in the presence of interfering compounds is summarized in **Figure 6A** and the original SWV data are displayed in **Figure S4**. The presence of all four interfering compounds in 2:1 ratio with the tested analyte doesn't interfere with peak, and resulted currents are not more than 10% different as exhibited in **Figure 6B**. Based on these results can be concluded that the established procedure could be considered as highly selective for the detection of trifluoperazine, and potentially usable for the determination of this drug when present in biological fluids.

Analysis of the real samples

To evaluate the detectability of the DMSA/Fe_3O_4/RGO/CNT sensor in actual testing, the standard recovery method was used to quantitatively analyze real urine and blood serum samples (**Figure S5**). The practical applicability of the procedure was investigated in four urine as well as two blood serum samples. Samples were processed following one of our previous works [45]. Recovery rates were investigated by two standard additions of TFP solution. Results were calculated from the calibration plots with three repetitive measurements and summarized in Table 2. Recovery rates of tested urine samples were in the range of 97.8%-101.6%, bias values were between -0.8% and 1.8% and the RSD in the range of 2.1%-3.5%. As for the blood serum tests, recovery rates were 98.9%-101.5%, bias was in the range of -1.7%-1.9% and the RSD were between 2.1% and 3.1%. The given values are the indicators of the accuracy of the method. These results demonstrate that the proposed DMSA/Fe_3O_4/RGO/CNT sensor possesses good reliability and feasibility for the detection of TFP in human urine and blood serum samples.

Table 2. Recovery data for spiked human urine and blood serum samples using DMSA/Fe_3O_4/RGO/CNT sensor.

	Sample	Detected (μM)	Addition 1			Addition 2			Recov. (%)
			Added* (μM)	Detected		Added* (μM)	Detected		
				Bias (%)	RSD (%)		Bias (%)	RSD (%)	
Urine	1	0.00	5.00	1.8	3.0	5.00	1.6	3.5	101.60
	2	0.00	5.00	-1.6	2.4	5.00	-1.2	2.6	97.80
	3	0.00	10.00	-1.1	2.1	10.00	-0.8	2.2	99.10
	4	0.00	10.00	-1.4	2.7	10.00	-1.6	2.8	98.40
Blood serum	1	0.00	5.00	-1.7	2.8	5.00	-1.9	3.1	98.9
	2	0.00	10.00	0.9	2.3	10.00	1.5	2.9	101.50

* Average of three replicate measurements.

Conclusions

Using an inkjet printing technology for highly reproducible CNT electrode fabrication and newly synthesized DMSA/Fe_3O_4/RGO nanocomposite for the electrode surface modification, an electrochemical sensor for the determination of trifluoperazine in biological fluids has been developed. A disposable, flexible, fast and easy to use sensor expressed a wide linear range of 1-50 μM, the submicromolar limit of detection of 0.54 μM, and excellent reproducibility and accuracy with negligible influence of potently interfering compounds. The here-presented results open new possibilities for the production of advanced miniature electrochemical devices for droplet-based detection of antipsychotic drug trifluoperazine founded on the utilization of state-of-the-art approaches. The future-related work will be directed toward the development of the portable "on body" sensing device, and transformation of the sensor for potential "on body" application. This perspective with excellent sensing properties may replace other more complicated and expensive methods in the foreseeable future.

Supporting information

The Supporting Information is available.

Cyclic voltammograms of bare and modified CTN electrodes at various scan rate

The electrochemical response of 10 μM of TFP under the same SWV conditions

The electrochemical response of TFP in the presence of different interfering compounds

The calibration plots used for real sample analysis

Corresponding Author

* M. Ognjanović E-mail Address: miloso@vin.bg.ac.rs the "Vinča" Institute of Nuclear Sciences, University of Belgrade, Mike Petrovića Alasa 12-14, 11001 Belgrade, Serbia

ORCID

Miloš Ognjanović: 0000-0003-2889-4416

Dalibor M. Stanković: 0000-0001-7465-1373

Milica Jović: 0000-0003-3495-2416

Andreas Lesch: 0000-0002-4995-2251

Hubert H. Girault: 0000-0001-5573-5774

Bratislav Antić: 0000-0002-5693-6401

Author Contributions

The manuscript was written through contributions of all authors

Notes

The authors declare no competing financial interest.

Acknowledgements

The authors like to thank Prof. M.P. Morales for help during the synthesis of nanoparticles. The authors gratefully acknowledge the support provided by the Ministry of Education, Science and Technological Development of the Republic of Serbia through Eureka project E!13303 MED-BIO-TEST.

References

(1) Hassan, A. K.; Ameen, S. T.; Saad, B.; Al-Aragi, S. M. Potentiometric Sensors for the Determination of Trifluoperazine Hydrochloride in Pharmaceutical Preparations. *Anal. Sci.* **2009**, *25*, 1295–1299.

(2) Gao, K.; Muzina, D.; Gajwani, P.; Calabrese, J. R. Efficacy of typical and atypical antipsychotics for primary and comorbid anxiety symptoms or disorders: a review. *The Journal of clinical psychiatry* **2006**, *67*, 1327–1340.

(3) Yeh, C.-T.; Wu, A. T. H.; Chang, P. M.-H.; Chen, K.-Y.; Yang, C.-N.; Yang, S.-C.; Ho, C.-C.; Chen, C.-C.; Kuo, Y.-L.; Lee, P.-Y.*; et al.* Trifluoperazine, an antipsychotic agent, inhibits cancer stem cell growth and overcomes drug resistance of lung cancer. *American journal of respiratory and critical care medicine* **2012**, *186*, 1180–1188.

(4) Srinivasan, S.; Chizmadzhev, Y. A.; Bockris, J. O.'M.; Conway, B. E.; Yeager, E. *Comprehensive Treatise of Electrochemistry*; Springer US: Boston, MA, 1985.

(5) *The United States Pharmacopeia : USP 24 : the National Formulary : NF 19 : by authority of the United States Pharmacopoeial Convention, Inc., meeting at Washington, D.C., March 9-12, 1995 ; prepared by the Committee of Revision and published by the Board of Trustees*; United States Pharmacopeial Convention: Rockville, Md., 1999.

(6) Stanković, D.; Dimitrijević, T.; Kuzmanović, D.; Krstić, M. P.; Petković, B. B. Voltammetric determination of an antipsychotic agent trifluoperazine at a boron-doped diamond electrode in human urine. *RSC Adv.* **2015**, *5*, 107058–107063.

(7) Jin, G.; Huang, F.; Li, W.; Yu, S.; Zhang, S.; Kong, J. Sensitive detection of trifluoperazine using a poly-ABSA/SWNTs film-modified glassy carbon electrode. *Talanta* **2008**, *74*, 815–820.

(8) Dogan-Topal, B. Electrooxidative behavior and determination of trifluoperazine at multiwalled carbon nanotube-modified glassy carbon electrode. *J Solid State Electrochem* **2013**, *17*, 1059–1066.

(9) A. Mohamed, M.; Saad, A. S.; Koshek, S. H.; El-Ghobashy, M. R. Smart electrochemical sensing platform for the simultaneous determination of psychotic disorder drugs isopropamide iodide and trifluoperazine hydrochloride. *New J. Chem.* **2018**, *42*, 9911–9919.

(10) Abd Muain, M. F.; Cheo, K. H.; Omar, M. N.; Amir Hamzah, A. S.; Lim, H. N.; Salleh, A. B.; Tan, W. S.; Ahmad Tajudin, A. Gold nanoparticle-decorated reduced-graphene oxide targeting anti hepatitis B virus core antigen. *Bioelectrochemistry (Amsterdam, Netherlands)* **2018**, *122*, 199–205.

(11) Georgakilas, V.; Perman, J. A.; Tucek, J.; Zboril, R. Broad family of carbon nanoallotropes: classification, chemistry, and applications of fullerenes, carbon dots, nanotubes, graphene, nanodiamonds, and combined superstructures. *Chemical reviews* **2015**, *115*, 4744–4822.

(12) Jariwala, D.; Sangwan, V. K.; Lauhon, L. J.; Marks, T. J.; Hersam, M. C. Carbon nanomaterials for electronics, optoelectronics, photovoltaics, and sensing. *Chemical Society reviews* **2013**, *42*, 2824–2860.

(13) Bahadır, E. B.; Sezgintürk, M. K. Applications of graphene in electrochemical sensing and biosensing. *TrAC Trends in Analytical Chemistry* **2016**, *76*, 1–14.

(14) Rather, J. A.; Pilehvar, S.; Wael, K. de. A graphene oxide amplification platform tagged with tyrosinase–zinc oxide quantum dot hybrids for the electrochemical sensing of hydroxylated polychlorobiphenyls. *Sensors and Actuators B: Chemical* **2014**, *190*, 612–620.

(15) Georgakilas, V.; Tiwari, J. N.; Kemp, K. C.; Perman, J. A.; Bourlinos, A. B.; Kim, K. S.; Zboril, R. Noncovalent Functionalization of Graphene and Graphene Oxide for Energy Materials, Biosensing, Catalytic, and Biomedical Applications. *Chemical reviews* **2016**, *116*, 5464–5519.

(16) Ding, D.; Maeyoshi, Y.; Kubota, M.; Wakasugi, J.; Kanamura, K.; Abe, H. Highly improved performances of LiMn0.7Fe0.3PO4

cathode with in situ electrochemically reduced graphene oxide. *Journal of Alloys and Compounds* **2019**, *793*, 627–634.

(17) Hasanzadeh, M.; Shadjou, N.; La Guardia, M. de. Iron and iron-oxide magnetic nanoparticles as signal-amplification elements in electrochemical biosensing. *TrAC Trends in Analytical Chemistry* **2015**, *72*, 1–9.

(18) He, J.; Yang, X.; Men, B.; Wang, D. Interfacial mechanisms of heterogeneous Fenton reactions catalyzed by iron-based materials: A review. *Journal of Environmental Sciences* **2016**, *39*, 97–109.

(19) Mohammed, L.; Gomaa, H. G.; Ragab, D.; Zhu, J. Magnetic nanoparticles for environmental and biomedical applications: A review. *Particuology* **2017**, *30*, 1–14.

(20) Zhang, L.; Wang, X.; Zou, J.; Liu, Y.; Wang, J. DMSA-Coated Iron Oxide Nanoparticles Greatly Affect the Expression of Genes Coding Cysteine-Rich Proteins by Their DMSA Coating. *Chemical research in toxicology* **2015**, *28*, 1961–1974.

(21) Ghalehno, M. H.; Mirzaei, M.; Torkzadeh-Mahani, M. Double strand DNA-based determination of menadione using a Fe3O4 nanoparticle decorated reduced graphene oxide modified carbon paste electrode. *Bioelectrochemistry (Amsterdam, Netherlands)* **2018**, *124*, 165–171.

(22) Su, X.; Chan, C.; Shi, J.; Tsang, M.-K.; Pan, Y.; Cheng, C.; Gerile, O.; Yang, M. A graphene quantum dot@Fe3O4@SiO2 based nanoprobe for drug delivery sensing and dual-modal fluorescence and MRI imaging in cancer cells. *Biosensors & bioelectronics* **2017**, *92*, 489–495.

(23) Stanković, D. M.; Ognjanović, M.; Espinosa, A.; del Puerto Morales, M.; Bessais, L.; Zehani, K.; Antić, B.; Dojcinović, B. Iron Oxide Nanoflower–Based Screen Print Electrode for Enhancement Removal of Organic Dye Using Electrochemical Approach. *Electrocatalysis* **2019**, *74*, 239.

(24) Wang, Q.; Zhang, X.; Huang, L.; Zhang, Z.; Dong, S. One-pot synthesis of Fe3O4 nanoparticle loaded 3D porous graphene nanocomposites with enhanced nanozyme activity for glucose detection. *ACS applied materials & interfaces* **2017**, *9*, 7465–7471.

(25) Aydogdu, M. O.; Ekren, N.; Suleymanoglu, M.; Erdem-Kuruca, S.; Lin, C.-C.; Bulbul, E.; Erdol, M. N.; Oktar, F. N.; Terzi, U. K.; Kilic, O. Novel electrospun polycaprolactone/graphene oxide/Fe3O4 nanocomposites for biomedical applications. *Colloids and Surfaces B: Biointerfaces* **2018**, *172*, 718–727.

(26) Jarošová, R.; Mcclure, S. E.; Gajda, M.; Jović, M.; Girault, H. H.; Lesch, A.; Maiden, M.; Waters, C.; Swain, G. M. Inkjet-Printed Carbon Nanotube Electrodes for Measuring Pyocyanin and Uric Acid in a Wound Fluid Simulant and Culture Media. *Analytical chemistry* **2019**, *91*, 8835–8844.

(27) Lesch, A.; Cortés-Salazar, F.; Amstutz, V.; Tacchini, P.; Girault, H. H. Inkjet printed nanohydrogel coated carbon nanotubes electrodes for matrix independent sensing. *Analytical chemistry* **2015**, *87*, 1026–1033.

(28) Qin, Y.; Kwon, H.-J.; Subrahmanyam, A.; Howlader, M. M.R.; Selvaganapathy, P. R.; Adronov, A.; Deen, M. J. Inkjet-printed bifunctional carbon nanotubes for pH sensing. *Materials Letters* **2016**, *176*, 68–70.

(29) Azoubel, S.; Shemesh, S.; Magdassi, S. Flexible electroluminescent device with inkjet-printed carbon nanotube electrodes. *Nanotechnology* **2012**, *23*, 344003.

(30) Stanković, D. M.; Ognjanović, M.; Jović, M.; Cuplić, V.; Lesch, A.; Girault, H. H.; Gavrović Jankulović, M.; Antić, B. Disposable Biosensor Based on Amidase/CeO2/GNR Modified Inkjet-printed CNT Electrodes-droplet Based Paracetamol Detection in Biological Fluids for "Point-of-care" Applications. *Electroanalysis* **2019**, *31*, 1517–1525.

(31) Stanković, D. M.; Jović, M.; Ognjanović, M.; Lesch, A.; Fabián, M.; Girault, H. H.; Antić, B. Point-of-care amperometric determination of L-dopa using an inkjet-printed carbon nanotube electrode modified with dandelion-like MnO2 microspheres. *Mikrochimica acta* **2019**, *186*, 532.

(32) Salas, G.; Casado, C.; Teran, F. J.; Miranda, R.; Serna, C. J.; Morales, M. P. Controlled synthesis of uniform magnetite nanocrystals with high-quality properties for biomedical applications. *J. Mater. Chem.* **2012**, *22*, 21065.

(33) Mejías, R.; Pérez-Yagüe, S.; Gutiérrez, L.; Cabrera, L. I.; Spada, R.; Acedo, P.; Serna, C. J.; Lázaro, F. J.; Villanueva, A.; Morales, M. D. P.*; et al.* Dimercaptosuccinic acid-coated magnetite nanoparticles for magnetically guided in vivo delivery of interferon gamma for cancer immunotherapy. *Biomaterials* **2011**, *32*, 2938–2952.

(34) Lu, T.; Pan, L.; Nie, C.; Zhao, Z.; Sun, Z. A green and fast way for reduction of graphene oxide in acidic aqueous solution via microwave assistance. *Phys. Status Solidi A* **2011**, *208*, 2325–2327.

(35) Schneider, C. A.; Rasband, W. S.; Eliceiri, K. W. NIH Image to ImageJ: 25 years of image analysis. *Nature Methods* **2012**, *9*, 671 EP -.

(36) Jović, M.; Zhu, Y.; Lesch, A.; Bondarenko, A.; Cortés-Salazar, F.; Gumy, F.; Girault, H. H. Inkjet-printed microtiter plates for portable electrochemical immunoassays. *Journal of Electroanalytical Chemistry* **2017**, *786*, 69–76.

(37) Lesch, A.; Cortés-Salazar, F.; Prudent, M.; Delobel, J.; Rastgar, S.; Lion, N.; Tissot, J.-D.; Tacchini, P.; Girault, H. H. Large scale inkjet-printing of carbon nanotubes electrodes for antioxidant assays in blood bags. *Journal of Electroanalytical Chemistry* **2014**, *717-718*, 61–68.

(38) Lesch, A.; Jović, M.; Baudoz, M.; Zhu, Y.; Tacchini, P.; Gumy, F.; Girault, H. H. (Invited) Point-of-Care Diagnostics with Inkjet-Printed Microchips. *ECS Trans.* **2017**, *77*, 73–81.

(39) Jović, M.; Cortés-Salazar, F.; Lesch, A.; Amstutz, V.; Bi, H.; Girault, H. H. Electrochemical detection of free chlorine at inkjet printed silver electrodes. *Journal of Electroanalytical Chemistry* **2015**, *756*, 171–178.

(40) Mehmeti, E.; Stanković, D. M.; Chaiyo, S.; Zavasnik, J.; Žagar, K.; Kalcher, K. Wiring of glucose oxidase with graphene nanoribbons: an electrochemical third generation glucose biosensor. *Microchim Acta* **2017**, *184*, 1127–1134.

(41) Lu, S.; Sui, L.; Liu, J.; Zhu, S.; Chen, A.; Jin, M.; Yang, B. Near-Infrared Photoluminescent Polymer-Carbon Nanodots with Two-Photon Fluorescence. *Advanced materials (Deerfield Beach, Fla.)* **2017**, *29*.

(42) Sun, S.; Guan, Q.; Liu, Y.; Wei, B.; Yang, Y.; Yu, Z. Highly luminescence manganese doped carbon dots. *Chinese Chemical Letters* **2019**, *30*, 1051–1054.

(43) Huízar-Félix, A. M.; Cruz-Silva, R.; Barandiarán, J. M.; García-Gutiérrez, D. I.; Orue, I.; Merida, D.; Sepúlveda-Guzmán, S. Magnetic properties of thermally reduced graphene oxide decorated with PtNi nanoparticles. *Journal of Alloys and Compounds* **2016**, *678*, 541–548.

(44) Stanković, D. M.; Ognjanović, M.; Martin, F.; Švorc, Ľ.; Mariano, J. F. M. L.; Antić, B. Design of titanium nitride- and wolfram carbide-doped RGO/GC electrodes for determination of gallic acid. *Analytical biochemistry* **2017**, *539*, 104–112.

(45) Vukojević, V.; Djurdjić, S.; Ognjanović, M.; Antić, B.; Kalcher, K.; Mutić, J.; Stanković, D. M. RuO2/graphene nanoribbon composite supported on screen printed electrode with enhanced electrocatalytic performances toward ethanol and NADH biosensing. *Biosensors & bioelectronics* **2018**, *117*, 392–397.

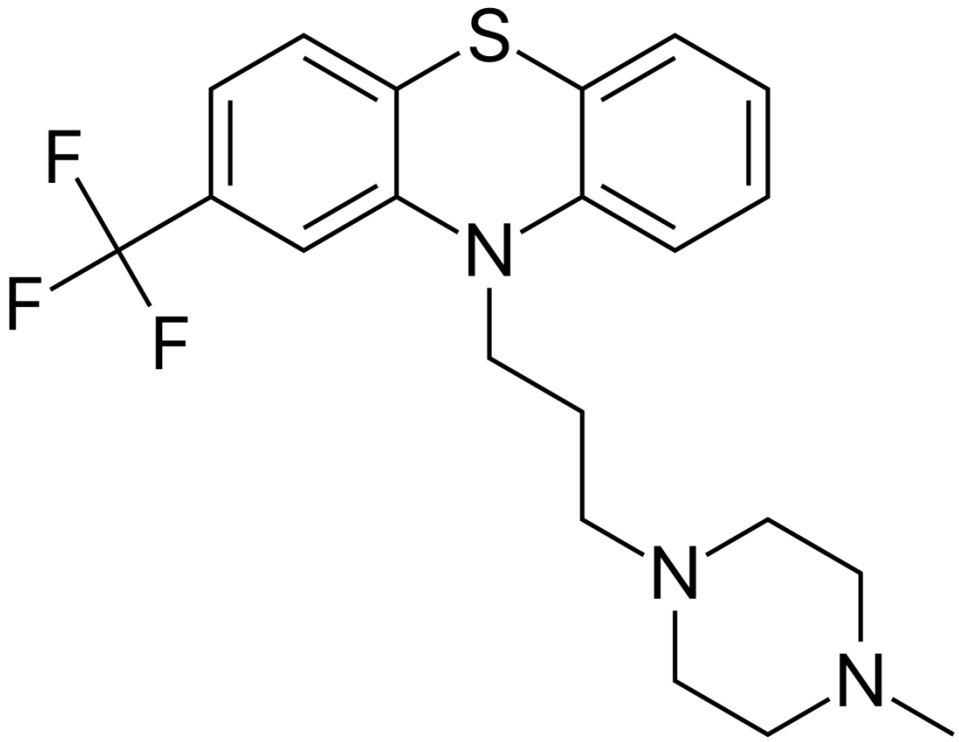

Scheme 1. 10-[3-(4-methyl-1-piperazinyl)propyl]-2-(trifluoromethyl)-10H-phenothiazine, (TFP).

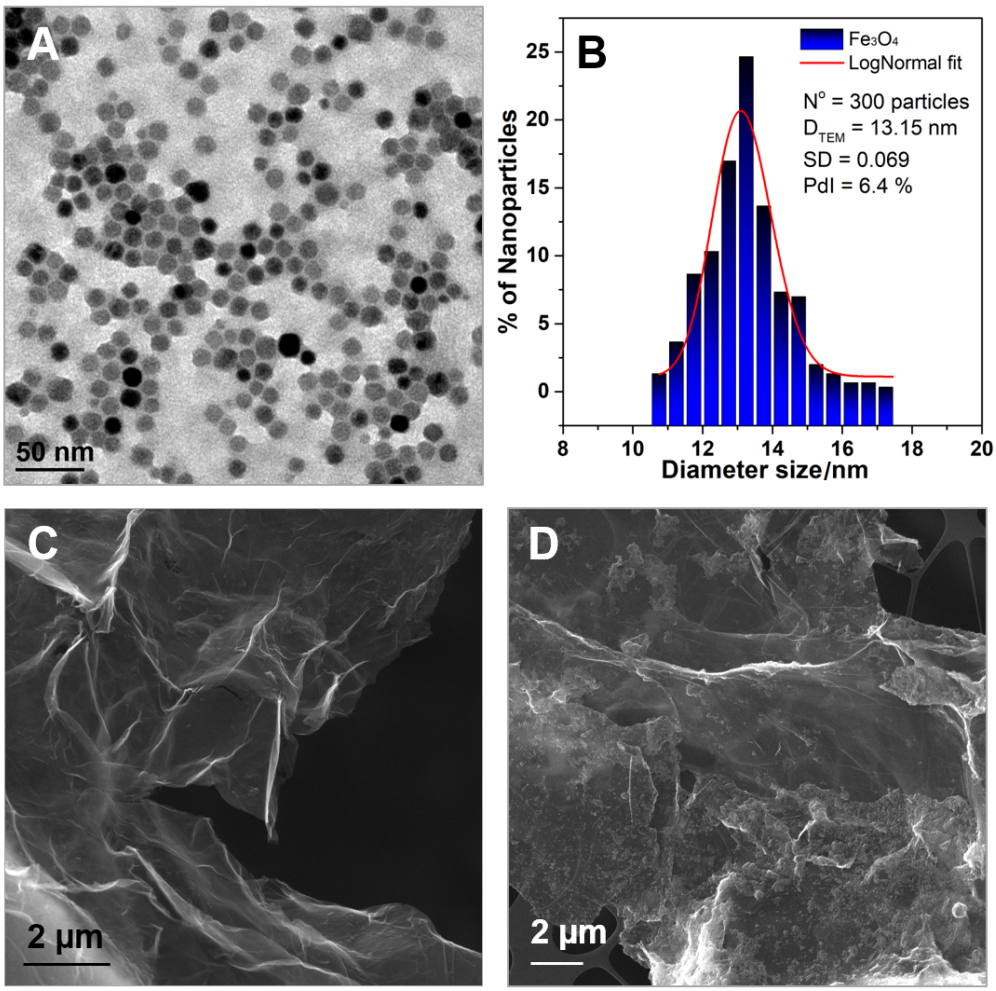

Figure 1. (A) TEM micrograph of DMSA coated Fe3O4 nanoparticles. Scale bar is 50 nm; (B) Log-normal size distribution of iron oxide nanoparticles; FE-SEM micrographs of (C) GO and (D) DMSA/Fe3O4/RGO nanocomposite.

284x280mm (96 x 96 DPI)

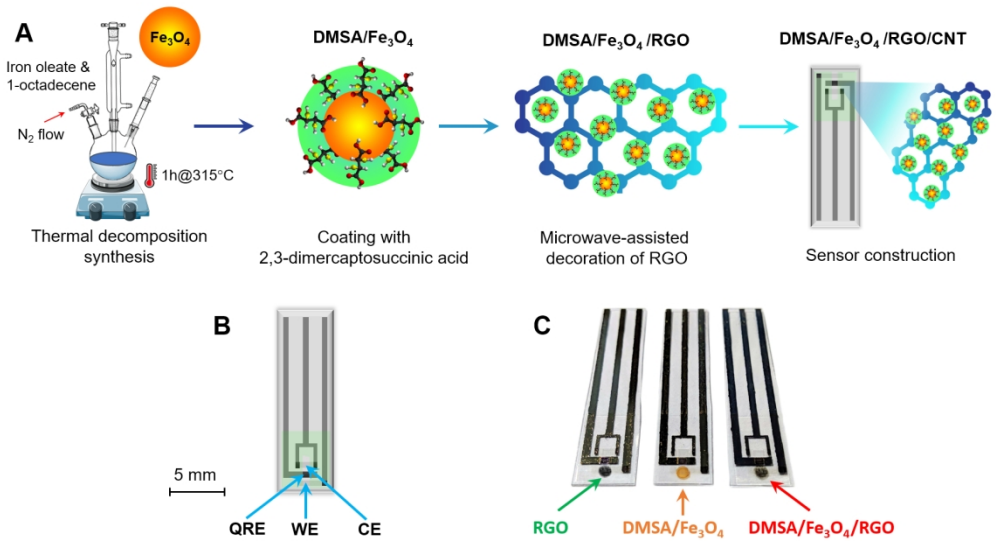

Scheme 2. (A) The synthesis of DMSA/Fe3O4/RGO nanocomposite and modification of CNT electrode (B) Schematic illustration of CNT electrode (QRE, WE and CE denote quasi-reference electrode, a working electrode and counter electrode, respectively); (C) Pho-tographs of three modified electrodes by drop-casting 2 μL of materials on working electrode.

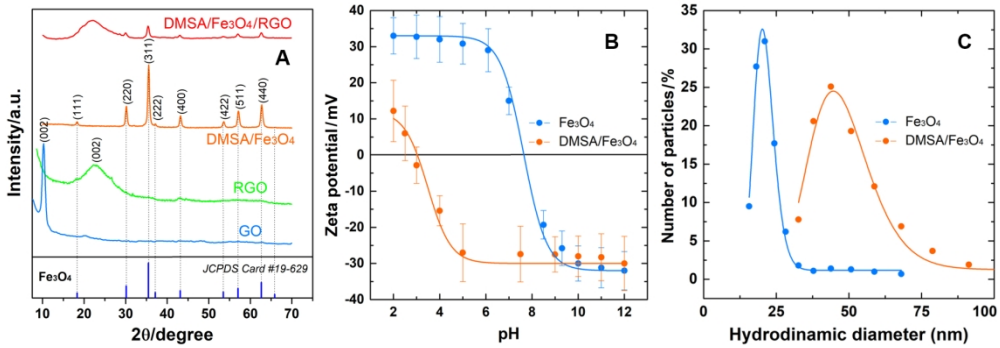

Figure 2. (A) XRPD patterns of the synthesized samples: GO (blue line), RGO (green line), DMSA/Fe3O4 nanoparticles (orange line) and DMSA/Fe3O4/RGO composite (red line). For comparison, a typical Fe3O4 pattern (JCPDS card #19-629) was displayed in the figure; B) The effect of pH on zeta potential of naked and DMSA coated Fe3O4 nanoparticles; (C) Hydrodynamic diameter of uncoated and coated nanoparticles.

408x141mm (120 x 120 DPI)

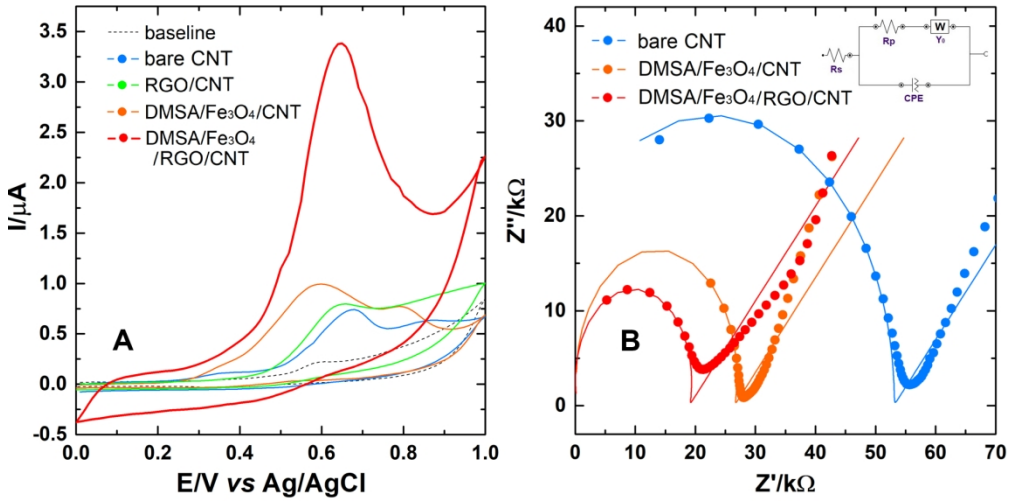

Figure 3. (A) Electrochemical response of TFP (75 μM) at bare CNT, DMSA/Fe3O4-, RGO- and DMSA/Fe3O4/RGO-modified CNT elec-trodes. Supporting electrolyte BRBS at pH 7, scan rate 50 mV·s-1; (B) Nyquist plots for various electrodes, bare CNT, RGO- DMSA/Fe3O4- and DMSA/Fe3O4/RGO-modified CNT. Inset: Equivalent circuit for the electrochemical impedance spectroscopy data. The frequency range was from 100 Hz to 100 kHz.

406x204mm (120 x 120 DPI)

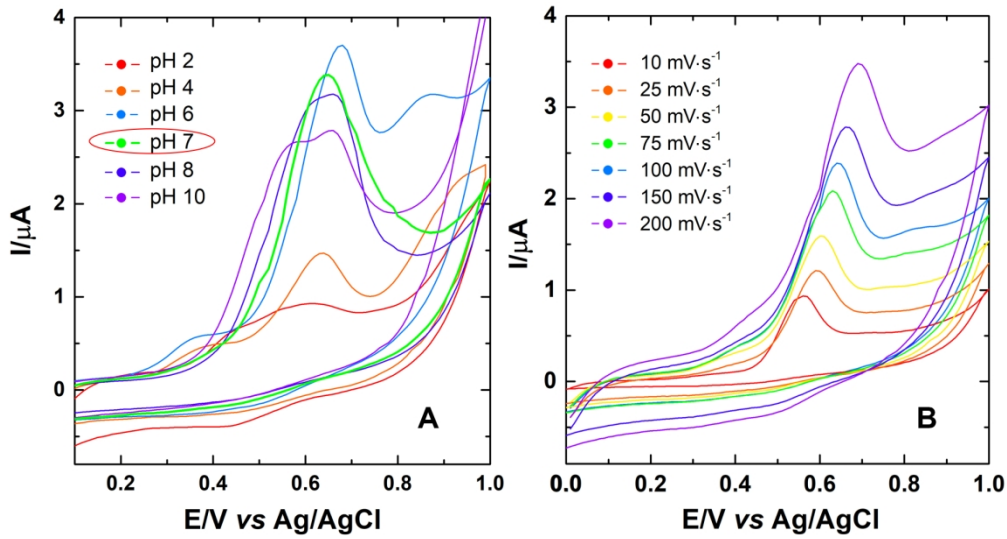

Figure 4. (A) Cyclic voltammograms of TFP (75 μM) at DMSA/Fe3O4/RGO-modified CNT electrode at various pH of BRBS. Scan rate 50 mV·s-1; (B) Cyclic voltammograms of TFP (75 μM) at DMSA/Fe3O4/RGO-modified CNT electrode at various scan rates. Supporting electrolyte BRBS pH 7.

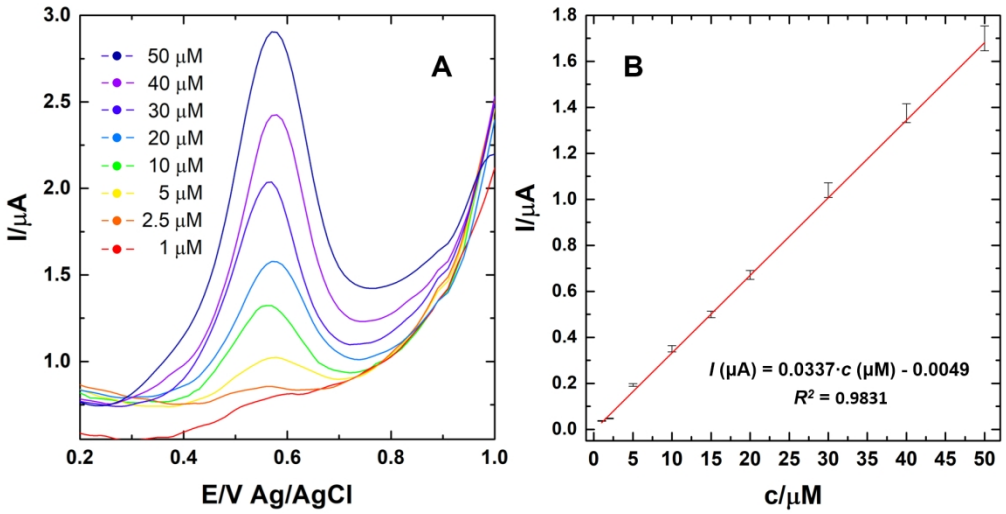

Figure 5. (A) SWV voltammograms obtained with DMSA/Fe3O4/RGO/CNT electrode for the concentration range of TFP from 1 to 50 μM, pH = 7; (B) Corresponding calibration plot evaluated from the measurements. All experiments were conducted under previously optimized experimental conditions.

406x207mm (120 x 120 DPI)

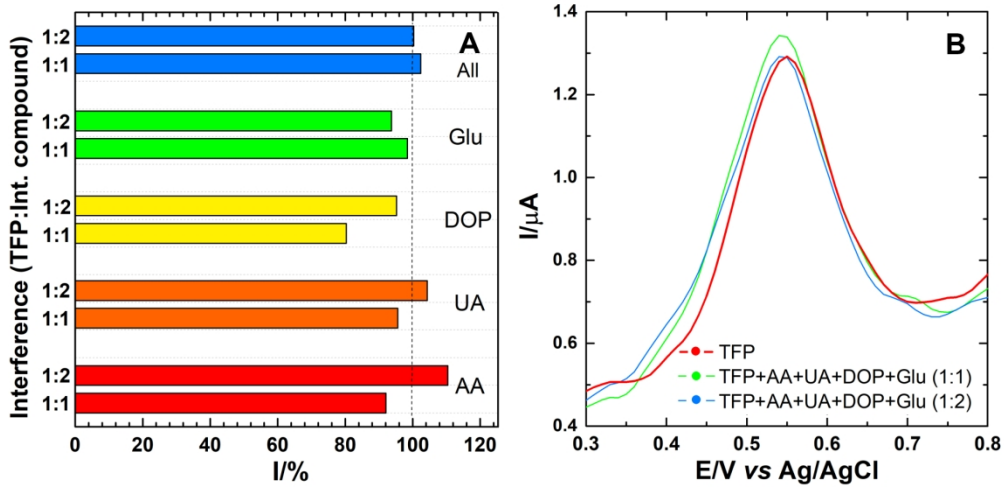

Figure 6. (A) Electrochemical response of TFP (10 μM) at DMSA/Fe3O4/RGO/CNT electrode in the presence of interfering com-pounds: ascorbic acid (AA), uric acid (UA), dopamine (DOP) and glucose (Glu) in concentration ration 1:1 and 1:2 v/v under optimized experimental conditions; (B) SWVs of the interference of all compounds combined.

508x248mm (96 x 96 DPI)

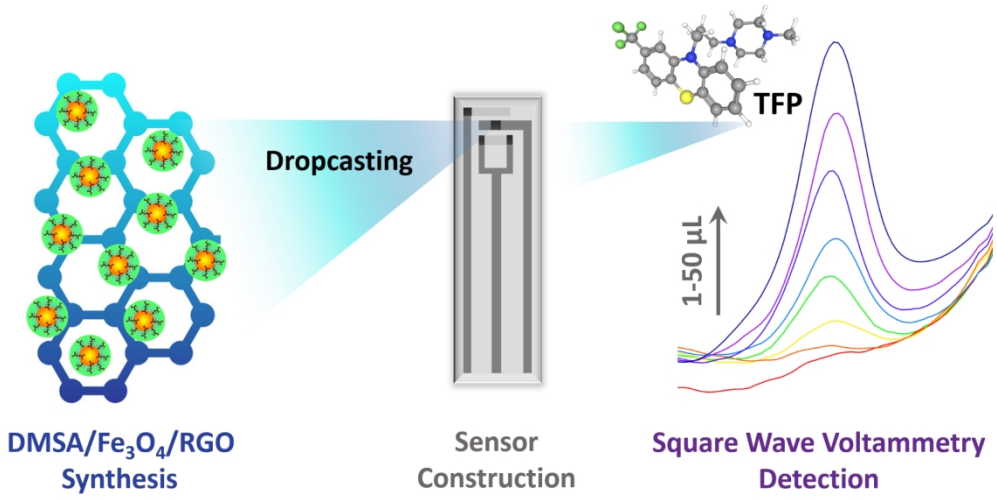

For Table of Contents Only

403x209mm (120 x 120 DPI)